Wetting Behavior of Water Droplets on Hydrophobic Microtextures of Comparable Size

Jürgen Jopp,[†] Holger Grüll,[‡] and Rachel Yerushalmi-Rozen*[,†,§]

The Ilse Katz Center for Meso- and Nanoscale Science and Technology and the Department of Chemical Engineering, Ben Gurion University in the Negev, 84105 Beer Sheva, Israel

Received January 26, 2004. In Final Form: August 3, 2004

The wetting behavior of water droplets on periodically structured hydrophobic surfaces was investigated. The effect of structure geometry, roughness, and relative pore fraction on the contact angles was investigated experimentally for droplets of size comparable to the size of the structures. It was found that surface geometry may induce a transition from groove-filling and Wenzel-like behavior to nonfilling of surface grooves and consequential Cassie−Baxter behavior. Numerical calculations of the free energy of these systems suggest that the equilibrium behavior is in line with the experimental observations. The observations may serve as guidelines for the design of surfaces with the desired wetting behavior.

Introduction

Wetting of rough surfaces is an old subject with many relevant questions still open.[1,2] One of the most common and practical issues is that of water droplets on nano- to microtextured hydrophobic surfaces:[3] Significant efforts were invested in the development of ultrarough surfaces via the development of surfaces with high surface area ratio (SAR), to impose high contact angles upon water droplets, leading to hydrophobicity and in some cases ultrahydrophobicity.[4−7] Yet, it was realized that the equilibrium contact angles of water droplets on a rough hydrophobic substrate often differ from the expected.[8,9] Namely, the measured (advancing) contact angle, θ, was found to be significantly lower than that predicted by the Wenzel relation[10] $\cos\theta_W = r\cos\theta_Y$, where θ_Y is the Young equilibrium contact angle on an ideal flat surface and r is the SAR or roughness factor, as it was originally called (r = (*actual suface*)/(*geometric surface*). The difference results from the ability of the air−substrate−water system to regulate the degree of penetration into surface grooves and to wet a heterogeneous substrate of air and solid (as schematically presented in Figure 1). The resulting contact angle may then be described by the Cassie−Baxter relation[11] $\cos\theta_{CB} = \phi_1\cos\theta_1 + \phi_2\cos\theta_2$, where ϕ_1 is the projected area fraction of the solid substrate, ϕ_2 is that of air, and θ_i are the respective Young contact angles. Thus, the system could minimize the overall free energy more efficiently than by the Wenzel route.

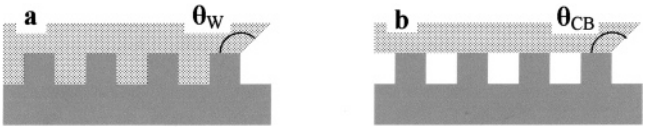

Figure 1. Schematic representation of a section from a large drop of liquid (the dotted area) on a textured surface. Two different cases are presented: (a) the pores are filled with liquid and (b) the drop rests on top of a composite surface of air patches (white areas) and solid (grey area).

Recently, there has been a renewed interest in the theoretical foundations of the Wenzel and Cassie relations.[12,13] Utilizing fundamental thermodynamic principles and applying methods for the minimization of the free energy under the relevant constraints, the effect of different surface topographies on the wetting behavior of droplets was addressed.

In this study, we investigate the wetting behavior of water droplets on periodic arrays of posts and pores produced via replication molding of a PDMS rubber. In particular, we examine the effect of structure geometry, roughness factor, r, and relative pore fraction, ϕ_2, on groove filling, and the consequential value of the contact angles of water droplets of size comparable to the size of the structures. We perform model calculations of the free energy of the system and compare the results with the experimental observations.

Experimental Section

Materials and Sample Preparation. Poly(dimethylsiloxane) (PDMS) stamps were prepared in a replication molding process using a 6-in. silicon wafer covered with a microstructured photoresist layer as a master. For preparation of the master, a 100-μm thick layer of photo resist (NanoTM SU-8, formulation 50−100, Microchem) is spin-coated on an acid-cleaned, hydrophilic silicon wafer. Subsequently, the photoresist is patterned with the desired features, using a printed foil mask. The master is pretreated for 15 min in an oxygen plasma and subsequently by a gas-phase surface modification for 60 min at a pressure of

* Author to whom correspondence should be addressed. E-mail: rachely@bgumail.bgu.ac.il.

[†] The Ilse Katz Center for Meso- and Nanoscale Science and Technology.

[‡] Philips Research Laboratories, Prof. Holstlaan 4, 5656 AA Eindhoven, The Netherlands.

[§] Department of Chemical Engineering.

(1) Öner, D.; McCarthy, T. J. *Langmuir* **2000**, *16*, 7777.
(2) Nakae, H.; Inui, R.; Hirata, Y.; Saito, H. *Acta Mater.* **1998**, *46*, 2313.
(3) Shiu, J.-Y.; Kuo, C.-W.; Chen, P.; Mou, C.-Y. *Chem. Mater.* **2004**, *16*, 561.
(4) Onda, T.; et al. *Langmuir* **1996**, *12*, 2125.
(5) Shibuichi, S.; et al. *J. Colloid Interface Sci.* **1998**, *208*, 287.
(6) Erbil, H. Y.; Demirel, A. L.; Avci, Y.; Mert, O. *Science* **2003**, *299*, 1377.
(7) Chen, W.; Fadeev, A. Y.; Hsieh, M. C.; Oener, D.; Youngblood, J.; McCarthy, T. J. *Langmuir* **1999**, *15*, 3395.
(8) Wolansky, G.; Marmur, A. *Colloids Surf. A* **1999**,*156*, 381.
(9) Bico, J.; Marzolin, C.; Quéré, D. *Europhys. Lett.* **1999**, *47*, 220
(10) Wenzel, R. N. *Ind. Eng. Chem.* **1936**, *28*, 988.
(11) Cassie, A. B. D.; Baxter, S. *Trans. Faraday Soc.* **1944**, *40*, 546.
(12) Swain, P. S.; Lipowsky, R. *Langmuir* **1998**, *14*, 6772.
(13) Marmur, A. *Langmuir* **2003**, *19*, 8343.

10.1021/la0497651 CCC: $27.50
Published on Web 10/14/2004

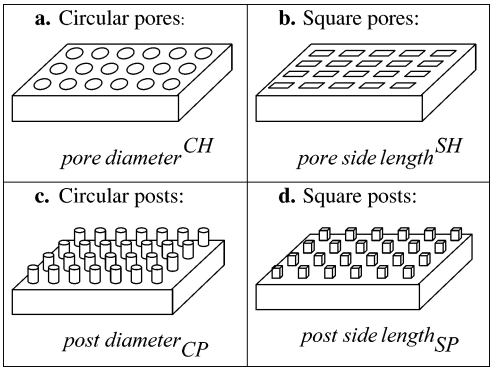

Figure 2. Sketches of the four types of microstructures used for the wetting experiments. The sample designation consists of two capital letters, indicating the topography, and a super- or subscript, which denotes for a given sample within a series the specific value of the diameter, d, of the circular posts or pores or the side length, s, of square post and pores, respectively.

approximately 0.1 mbar with 1H,1H,2H,2H-perfluorodecyltrichlorosilane (ABCR, D-76189 Karlsruhe, Germany) followed by a baking step of 30 min at 100 °C. The pretreated master is placed in a holder, and a degassed silicone mixture is poured over it (SYLGARD 184 elastomer and curing agent, in a weight ratio of 10:1, Dow Corning). The polymer is allowed to cure for 24 h at 60 °C and cooled to room temperature before being removed from the master. Prior to the wetting experiments, the samples were cleaned from dust with nitrogen gas. Millipore water (10^{18} Ω cm) was used for wetting experiments.

Characterization Methods. *Contact-Angle Measurements.* A Ramé−Hart telescopic goniometer, equipped with CCD camera, was used to measure advancing and receding contact angles. Receding angles were measured by withdrawing liquid from the droplet. We report the median value (typically 3−5 measurements) of the advancing and receding contact angles for water droplets of a typical volume of 10 μL.

Groove Filling. Two methods were used to determine groove filling: visual inspection of the sample and contact-angle hysteresis. When liquid was withdrawn from droplets, the contact angles were either similar to those of the advancing angles, showing low hysteresis, or the angles were significantly lower than the advancing angles (by 50°−60°) and became lower as the droplet volume was further reduced.[14] In the latter systems, the value of the contact angle did not reach a steady state (which in this limit is complete wetting). The first behavior served as an indication for the "nonfilled" regime, while the second type of behavior indicated that the structures are filled by water.

Electron Microscopy. SEM images of the different structures were taken at 300× magnification using a JSM-35CF of JEOL, operated at 15 kV. For SEM, the samples were coated with a few nanometers of sputtered gold. Optical microscopy in the reflectance mode (Zeiss SV11, coupled to a computer controlled CCD camera) was used to characterize quantitatively the structured surfaces.

Sample Characterization. Four series of microstructures were investigated: pores and posts of a circular-shaped cross-section, and pores and posts of a square-shaped cross-section. We identify them by two capital letters, representing their respective topography (Figure 2). The microstructures are arranged on a quadratic grid with a nearest-neighbor center-to-center distance of 250 μm for circular shapes and 200 μm for square shapes. The depth of each of the pores is 110 μm, and the height of each of the posts is 100 μm. Different samples within a series vary only in the diameter, or side length, of the cross-section of the pores or posts, in the range of 40−150 μm.

The diameter, d, of circular posts or pores, the side-length, s, of square post or pores, and the center-to-center distance, l, between a pore (or post) and its nearest neighbor were measured using top-view images. The height of the posts and the depth of the pores, h, were measured from cross-sectional images. The measured values were used for calculating the following relations: (1) Pore fraction $\phi_2 = d^2\pi(2l)^{-2}$ for circular pores, and $\phi_2 = s^2l^{-2}$ for square pores, solid fraction $\phi_1 = d^2\pi(2l)^{-2}$ for circular posts, and $\phi_1 = s^2l^{-2}$ for square posts. Note that for each structure the solid fraction and the pore fraction are related via the relation $\phi_1 = 1 - \phi_2$. (2) The surface area of the sidewalls $A_s = d\pi h$ for circular structures and $A_s = 4sh$ for square structures. (3) The roughness factor $r = (l^2 + A_s)l^{-2}$.

We refer to the volume of the pores and of the gap between the posts as pore volume. The different samples were also characterized by SEM. In Figure 3, we present SEM images of a surface with cylindrical posts of 120-μm diameter and of a surface with cylindrical pores of 130-μm diameter.

Table 1. Surface Texture of Microstructured PDMS Surfaces and Wetting Behavior of a Water Droplet

no.	surface topography	roughness factor, r	pore fraction, ϕ_2 (in %)	groove filling	θ_{adv} (deg) ± 2	θ_{re} (deg) ± 5
1	smooth	1	0		100	75
2	$_{90\mu m}CH$	1.5	10	No	99	94
3	$_{110\mu m}CH$	1.61	15	No	102	106
4	$_{130\mu m}CH$	1.72	21	No	103	92
5	$_{150\mu m}CH$	1.83	28	No	109	97
6	$_{80\mu m}SH$	1.88	16	No	111	76
7	$_{120\mu m}SH$	2.32	36	No	108	84
8	$^{120\mu m}CP$	1.6	82	Yes	127	
9	$^{100\mu m}CP$	1.5	87.5	Yes	129	
10	$^{80\mu m}CP$	1.4	92	Yes	126	
11	$^{60\mu m}CP$	1.3	95.5	Yes	113	
12	$^{80\mu m}SP$	1.8	84	No	123	124
13	$^{40\mu m}SP$	1.4	96	Yes	115	

Results and Discussion

In this study, we investigated the wetting behavior of water droplets on regularly structured hydrophobic PDMS surfaces. The samples were designed to exhibit a roughness factor ranging from 1 (smooth surface) to 2.32 (rough surface) and a pore fraction from 0% to 96%. High pore fractions were attained in structures formed by well-separated posts. These structures were complemented by surfaces of similar roughness factor, but low pore fraction, attained by replacing posts by pores of similar dimensions. Thus, by changing the geometry, it was possible to decouple the two parameters. In Table 1, we present the calculated roughness factor and the pore fraction for each of the structures. The table further denotes the characteristic wetting behavior: the pore filling and the experimentally measured contact angles (CA) of water on the different surfaces.

We observe that surfaces of similar roughness factor may exhibit advancing CA that differ by 30° (e.g., the experiments described in line 2 and line 9 of Table 1), while surfaces of very different roughness factor (1.83 and 2.32) may exhibit similar advancing CA (109° and 108°, respectively, in lines 5 and 7). We also find that surfaces that differ by the value of the pore fraction exhibit similar advancing CA (see lines 6 and 11). Note as well that all the post structures (except the sample described in line 12) are in the filling regime, while all the pore structures are not. We only report receding contact angles values for the nonfilled structures as the droplets spread on top of the filled grooves. As described in the Experimental Section, we actually use the behavior of the receding angles as an additional indication (besides visual inspection) for the wetting regime—low hysteresis indicates that the structure is in the nonfilling regime, while high hysteresis and inability to attain a steady-state value of the receding contact angle is taken as an indication for groove filling. Note that the contact-angle hysteresis is larger for the

(14) Lafuma, A.; Quéré, D. *Nat. Mater.* **2003**, *2*, 457.

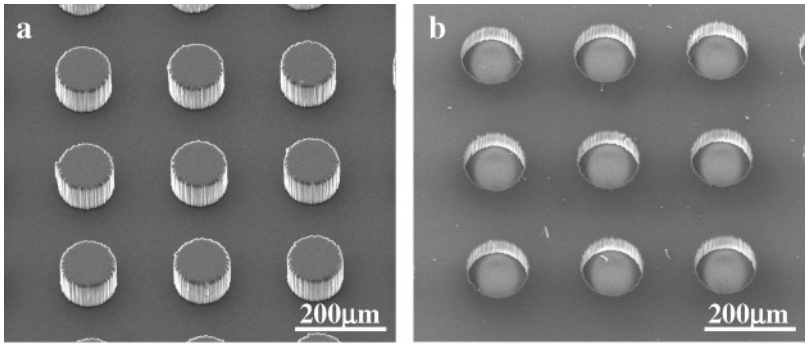

Figure 3. SEM images (a) of the structures $^{120\mu m}CP$, standing cylindrical posts of 120 μm diameter at a tilt angle of 30° and (b) of $_{130\mu m}CH$, cylindrical pores of 130 μm diameter at a tilt angle of 20°. The scale bar is 200 μm in both images

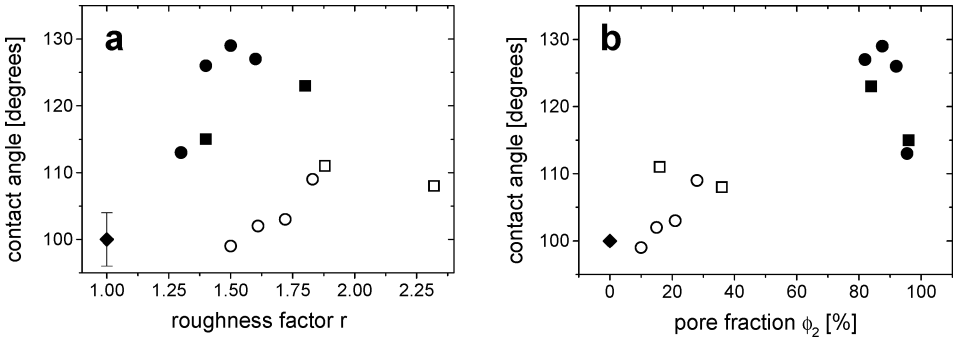

Figure 4. Contact angle of water droplets (typical volume of 10^{10} μm^3) for structures presented in Table 1 as a function of (a) the roughness factor and (b) the pore fraction. The symbols relate to the types of surfaces: SP, ■; CP, ●; SH, □; CH, ○; and the smooth surface, ◆.

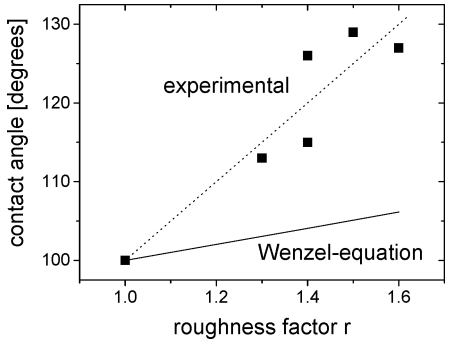

Figure 5. Contact-angle values of water droplets on structures 8−11 and 13 (Table 1) as a function of the roughness factor, r. The dotted line is a guide to the eye. The calculated Wenzel relation and the value found on a smooth surface (line 1, Table 1) are depicted for comparison.

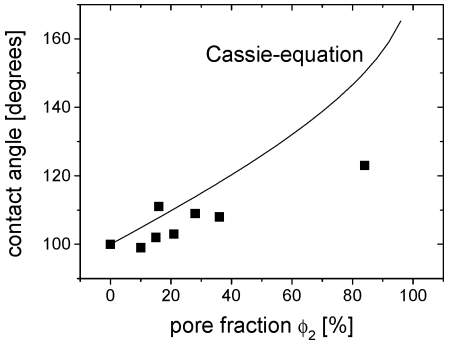

Figure 6. Contact-angle values of water droplets on structures 1−7 and 12 (Table 1) as a function of the pore fraction. The calculated Cassie relation and the value of the smooth surface (line 1, Table 1) are depicted for comparison.

SH structures (Table 1 lines 6, 7) as compared to the CH structures. An important observation is that the advancing angles are below 130°, even for structures characterized by high roughness factors, unlike small-scale structures, where values of 160−175°, were reported.[14]

In Figure 4, we present the advancing CA as a function of the roughness factor (Figure 4a) and pore fraction (Figure 4b).

In Figure 5, we present the CA measured for water-filled grooves as a function of r and, in Figure 6, the CA of droplets that do not fill the grooves as a function of pore fraction.

Regrouping highlights the characteristic dependence of each subgroup: in one case, the data show that the contact angle increases with the roughness factor, r (Figure 5), and in the other case, the CA increases with the pore fraction, as predicted by CB (Figure 6), but the fit is not quantitative. We show further that this is a consequence of the large size of the structures.

We note, however, that the dependence of the CA on the roughness factor, r (Figure 5), is stronger than predicted, and while the Cassie−Baxter equation is able to predict the observed trend for the measured contact angles, those values are generally smaller, and the deviation increases with increasing pore fraction.[8]

Observations of a transition from Wenzel to Cassie−Baxter behavior were reported before. Yet, these transitions were often attributed to pinning of the contact line or uncontrolled surface heterogeneities.[15] Here, we follow the suggestion[13] that a thermodynamic transition from groove-filling to nonfilling is the origin of the observed behavior.

Following the notation presented by Marmur,[13] we performed a numerical calculation of the Gibbs free energy of the system, as a function of the apparent contact angle, θ, and the penetration depth, z, of the liquid into the pores.

(15) Yoshimitsu, Z.; Nakajima, A.; Watanabe, T.; Hashimoto, K. *Langmuir* **2002**, *18*, 5818.

We restate eqs 3−7 of ref 13:

$$G = \sigma_{lf}A_{lf} + \sigma_{sl}A_{sl} + \sigma_{sf}A_{sf} \quad (1)$$

$$A_{lf} = 2\pi R^2(1 - \cos\theta) + (1 - f)\pi R^2 \sin^2\theta \quad (2)$$

$$A_{sl} = \pi R^2 r_f f \sin^2\theta \quad (3)$$

$$A_{sf} = [A_{tot} - \pi R^2 r \sin^2\theta] + \pi R^2 r_{1-f}(1 - f)\sin^2\theta \quad (4)$$

$$r_f f + r_{1-f}(1 - f) = r \quad (5)$$

G is the Gibbs energy of the system, σ is the interfacial tension of the relevant interface, A is the interfacial area, and the subscripts s, l, and f stand for the solid, liquid, and fluid, respectively (which in our system are PDMS, water, and air, respectively). R is the radius of the drop, θ its apparent contact angle, f is the fraction of the projected area that is wet by the liquid, r is the roughness factor, r_f and r_{1-f} are the roughness factors of the wet and dry area.

For the samples investigated here, the side walls are vertical and the penetration depth, z, ranges from $z = 0$ at the top surface to $z = h$ at the bottom surface, thus $r_f(z)$ is given by $r_f(0) = 1$, $r_f(h) = r$, and $r_f(z) = 1 + \Delta r_f z$ for $0 < z < h$, with $\Delta r_f = 4s^{-1}$ for SP structures, $\Delta r_f = 4d^{-1}$ for CP structures, $\Delta r_f = 4s(l^2 + s^2)^{-1}$ for SH structures and $\Delta r_f = d\pi(l^2 + 0.25d^2\pi)^{-1}$ for CH structures. Because of the vertical side walls, the function $f(z)$ is a step-function, with a constant value of $f(z) = \phi_1$, for $z < h$ and $f(h) = 1$.

In ref 13, it is assumed that the volume of the liquid trapped in the grooves is negligible as compared to the drop volume. In our case, the pore volume is non-negligible and may approach up to 8% of a typical drop volume. The largest pore volume is found for the structure $^{40\mu m}SP$. For a droplet volume of 10^8 μm^3, 10^{10}, and 10^{14} μm^3, the volume fraction of the filled pores amounts to 30.6%, 8%, and 0.4%, respectively. To take account of that, we modify the equations.

The volume of the pores which is filled by the liquid, is $V_p = (1 - \phi_1)R^2\pi z \sin^2\theta$, assuming a planar liquid vapor interface inside the pores.[16] The volume of the drop is given by $V_{drop} = (2 - 3\cos\theta + \cos^3\theta)R^3\pi/3$ and $V_0 = V_p + V_{drop}$ is the total volume of the liquid phase.

The modified expression for the normalized Gibbs free energy becomes[17]

$$G^* \equiv \frac{G - \sigma_{sf}A_{tot}}{\sigma_{lf}\pi^{(1/3)}(3V_0)^{(2/3)}} = \left(1 - \frac{V_p}{V_0}\right)^{2/3}(2 - 3\cos\theta + \cos^3\theta)^{-2/3}[2 - 2\cos\theta - (r_f f\cos\theta_Y + f - 1)\sin^2\theta] \quad (6)$$

We evaluate[18] this equation for a parameter field of $0 \le z \le h$ in steps of 1 μm and $90° < \theta < 180°$ in steps of 1°. (Note that the drop radius, R, which appears as a parameter in the equations for V_p and V_{drop}, is indirectly fixed by the total volume V_0). The main results are demonstrated in Figure 7.

(16) While this assumption does not affect the shape of the function, it modifies the predicted value of the contact angle.

(17) For negligible pore volume $V_p = 0$ and $A_{tot} = 0$, the equations become identical to eqs 9−11 of ref 13

(18) We used Microsoft Excel for these calculations: we specify f, r_f, and h for a given sample. We use the measured Young contact angle $\theta_Y = 100°$, and start from an estimate for R (typically about 1000 μm). The program then calculates V_p, V_{drop}, V_0, and G^*. We then specify the desired value for the total volume of the liquid-phase V_0 (e.g., 10^{10} μm^3) and use the "goalseek" function of Excel to adjust the drop radius, R. All other results, in particular, G^*, are updated simultaneously.

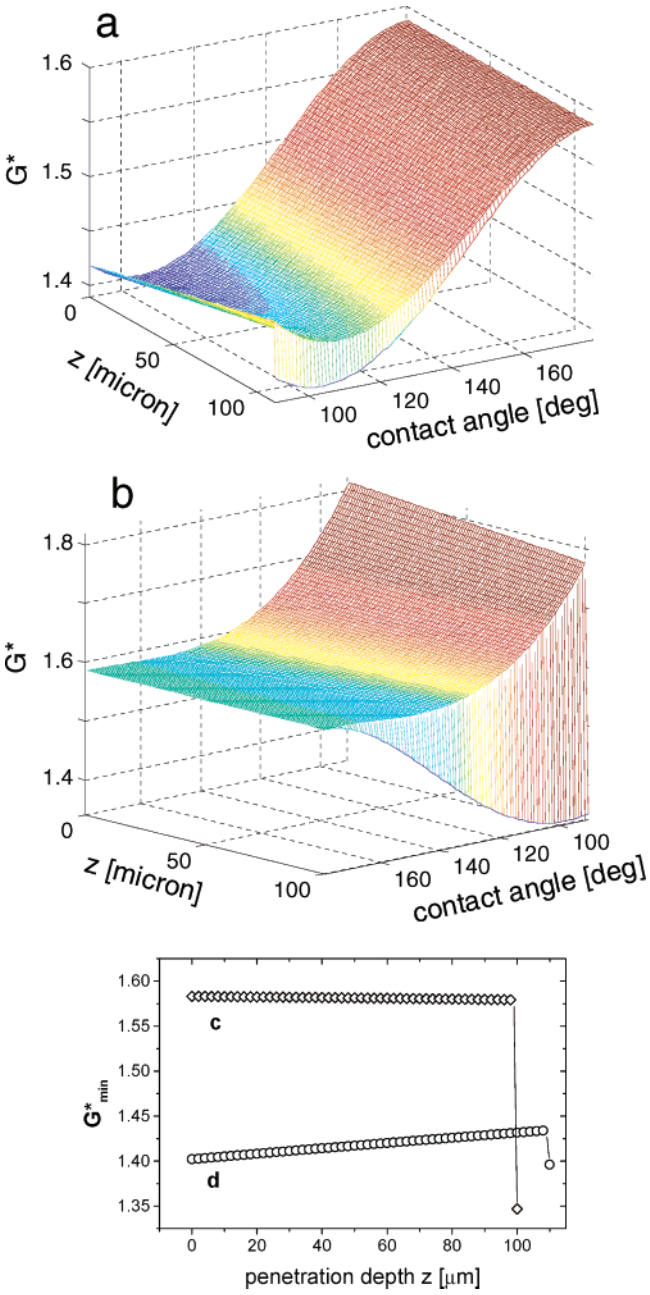

Figure 7. 3D plots of the normalized free energy $G^*(z, \theta)$ for the exemplary samples (a) $_{90\mu m}CH$ and (b) $^{100\mu m}CP$. For both samples, we also show 2D graphs (c, d) of $G^*_{min}(z)$, the minimal values of G^* for a given penetration depth z. For the pore structure (a, d), a Cassie minimum at a penetration depth $z = 0$ is visible, whereas for the post structure (b, c), no Cassie minimum is found. (The calculations were made for a drop volume of 10^{10} μm^3.)

For a droplet volume of 10^{10} μm^3 (which is about the experimental value), we observe two distinct behaviors.

(a) Pores (circular and square, different dimensions): we observe that the Gibbs free energy, G^*, exhibits a local minimum for $z = 0$ followed by an increase in G^* with higher values of z. This behavior disfavors penetration of liquid into the pores and suggests that the wetting behavior may be well described by the Cassie-relation.

(b) Posts (circular and square, different dimensions): a monotonic decrease of G* as a function of z is observed, as well as a single minimum for completely filled pores, suggesting that the wetting behavior may be described by the Wenzel relation. This behavior is consistent with the experimental observations: we observe groove filling and

homogeneous wetting in "post" structures (Table 1, lines 8−11 and 13), and droplets on top of the air-filled grooves in "pore" structures (Table 1, lines 1−7). An interesting observation is related to the structure $^{80\mu m}SP$. Though this structure is an array of square posts, a Cassie minimum was found in the calculations with the specified drop volume, indicating that the lower energy state is that of droplets that do not fill the grooves. Indeed, the experiments (Table 1, line 12) showed clearly that water droplets did not fill the grooves. The ability of the model to predict the observed transition in the wetting behavior (from groove filling to nonfilling) increases our confidence in the validity and relevance of the model to the description of this type of systems.

The origin of the observed dependence of the contact angle on droplet size was investigated in different studies.[8,19] Here, we tested the effect of droplet size on the local and global minima of the free energy for each surface structure. G^* was calculated for droplet volume $V_0 \rightarrow \infty$ (which implies that the fraction of the liquid within the pores becomes negligible) and for $V_0 \rightarrow 0$.[20] We find that in the case $V_0 \rightarrow \infty$ a minimum in the free energy, G^*, at $z = 0$ exists regardless the type of surface structure, suggesting that the systems may be described by the Cassie−Baxter relation. When $V_0 \rightarrow 0$, we find that for some structures the calculated Wenzel contact angle is smaller than the Young contact angle. This unphysical result may indicate that, for the structures investigated by us, some of the assumptions made in the derivation of the Wenzel relation are no longer adequate. For example, in the Wenzel equation, only the increased interfacial area between the liquid and the solid is accounted for, whereas the additional liquid−air interface in the pores is neglected. For small droplets, that latter should be accounted for. By small size droplets (relative to the scale of the surface structures), an effective roughness factor, as well as surface composition (PDMS-to-air ratio), is experienced, leading to a strong dependence of the contact angle on droplet diameter. In addition, in such cases, we expect the CA to be sensitive to the local minima of the free energy. This implies that the measured values are sensitive to experimental details, such as the way of deposition, and on the place where the drop is deposited. Indeed, we observe, in some cases, a large variability in the values of the CA (on a given surface). Furthermore, the shape of the three-phase contact line and the shape of the liquid−fluid interface deviate from circular and hemispherical shapes due to distortions induced by surface structures. Thus, the validity of G^*, as described in eq 6, to small droplets is limited, as was thoroughly discussed before.[8,21]

To summarize, we observed that the wetting behavior of water droplets on hydrophobic surface structures of similar dimensions is sensitive to the details of the geometry due to the ability of the system to optimize the ratio between the free energy cost of wetting a patchy air−PDMS substrate versus the consequential increase in the roughness. The balance of these energy terms determines whether the system will be found in the regime of so-called heterogeneous or homogeneous wetting.[13] In particular, we found that homogeneous wetting and the consequential Wenzel-type behavior are observed for post structures with sufficiently high pore fraction, while in the case of pores, water droplets do not penetrate into the grooves and heterogeneous wetting takes place, leading to a contact-angle dependence of the Cassie-type. The agreement between the experimental observations and the free energy calculations presented here suggest that free energy calculations may serve as an efficient tool for rational design of hydrophobic surfaces with predetermined wetting behavior.

Supporting Information Available: 2D graphs of $G^*_{min}(z)$, the minimal values of G^* for a given penetration depth, z, calculated for each structure for droplet volumes of 10^8, 10^{10}, and 10^{14} μm^3. This material is available free of charge via the Internet at http://pubs.acs.org.

LA0497651

(19) Checco, A.; Guenoun, P.; Daillant, J. *Phys. Rev. Lett.* **2003**, *91*, 186101.

(20) We calculated G^* for all samples for a drop size of 10^8, 10^{10}, and 10^{14} μm^3.

(21) Brandon, S.; Haimovich, N.; Yeger, E.; Marmur, A. *J. Colloid Interface Sci.* **2003**, *263*, 237.